

## Line-Node Dirac Semimetal and Topological Insulating Phase in Noncentrosymmetric Pnictides $\text{CaAgX}$ ( $X = \text{P, As}$ )

Ai Yamakage,<sup>1,3</sup> Youichi Yamakawa,<sup>2,3</sup> Yukio Tanaka,<sup>1</sup> and Yoshihiko Okamoto<sup>1,3</sup>

<sup>1</sup>*Department of Applied Physics, Nagoya University, Nagoya 464-8603, Japan*

<sup>2</sup>*Department of Physics, Nagoya University, Nagoya 464-8602, Japan*

<sup>3</sup>*Institute for Advanced Research, Nagoya University, Nagoya 464-8601, Japan*

Two noncentrosymmetric ternary pnictides,  $\text{CaAgP}$  and  $\text{CaAgAs}$ , are reported as topological line-node semimetals protected solely by mirror-reflection symmetry. The band gap vanishes on a circle in momentum space, and surface states emerge within the circle. Extending this study to spin-orbit coupled systems reveals that, compared with  $\text{CaAgP}$ , a substantial band gap is induced in  $\text{CaAgAs}$  by large spin-orbit interaction. The resulting states are a topological insulator, in which the  $\mathbb{Z}_2$  topological invariant is given by 1;000. To clarify the  $\mathbb{Z}_2$  topological invariants for time-reversal-invariant systems without spatial-inversion symmetry, we introduce an alternative way to calculate the invariants characterizing a line node and topological insulator for mirror-reflection-invariant systems.

**Introduction.**— The idea of topology has been greatly expanded in the field of condensed matter physics. The quantum Hall effect can be viewed as a topological insulating state.<sup>1,2</sup> In the past decade, various topological insulators respecting time-reversal symmetry have been discovered and this has motivated numerous subsequent studies.<sup>3–5</sup> However, zero-gap semiconductors (Weyl/Dirac semimetals)<sup>6–9</sup> have recently been recognized as a topologically nontrivial system. The absence of a band gap and the approximately linear dispersion in the low-energy regime are the characteristic features of the Weyl/Dirac semimetals. Because the low-lying excitations are the same as those of relativistic massless fermions, i.e., Weyl/Dirac fermions, anomalous transport phenomena such as the chiral magnetic effect<sup>10</sup> can be expected not only in high-energy physics but also in solids.<sup>11,12</sup> Thus, exploring topological semimetals can serve as a basis for understanding novel phenomena in condensed matter physics.

In most Weyl/Dirac semimetals, conduction bands overlap with valence bands at certain momentum points. However, the band gap rarely vanishes on a momentum line.<sup>13–16</sup> Such a dispersion structure is called a “line node,” which is analogous to that in line-node superconductors. Recently, many systems have been proposed as line-node semimetals (e.g., graphite,<sup>17–19</sup> the heterostructure of topological insulators,<sup>20</sup> hyperhoneycomb lattice,<sup>21</sup> transition-metal monophosphides,<sup>22</sup> carbon allotropes,<sup>23,24</sup>  $\text{Cu}_3\text{N}$ ,<sup>25</sup> antiperovskites,<sup>26</sup> rare-earth monopnictides,<sup>27</sup> and perovskite iridates<sup>28–31</sup>). Furthermore, several quantum phenomena are also expected to appear in line-node semimetals; these include a flat Landau level,<sup>32</sup> long-range Coulomb interaction,<sup>33</sup> the Kondo effect,<sup>34</sup> and a quasi-topological electromagnetic response that induces charge polarization and orbital magnetization proportional to the length of the line node.<sup>35</sup> Experimental results on line-node semimetal materials are also being reported.<sup>36–38</sup> Interestingly, in addition to these materials, photonic crystals<sup>39</sup> and

spin liquids<sup>40</sup> have been shown to host line nodes. The line-node structure of energy bands is becoming a prominent topic.

In this Letter, we propose hexagonal pnictides  $\text{CaAgX}$  ( $X = \text{P}$  and  $\text{As}$ ) as novel line-node Dirac semimetals. Mewis synthesized these compounds and found that they crystallize in the  $\text{ZrNiAl}$ -type structure with space group  $\text{P}\bar{6}2\text{m}$ .<sup>41</sup> As depicted in Fig. 1(a),  $\text{AgX}_4$  tetrahedra form a three-dimensional network by sharing their edges and corners with intervening  $\text{Ca}$  atoms, which form a kagome-triangular lattice.<sup>42</sup> An important aspect of this structure in terms of the physics of topology is that the space group has  $\text{D}_{3\text{h}}$  point-group symmetry, i.e., mirror-reflection symmetry is preserved while spatial-inversion symmetry is not, although almost all of the previously studied line-node semimetal materials have spatial-inversion symmetry. First-principles calculations and symmetry consideration indicate that there actually exists a line-node in  $\text{CaAgX}$ . Additionally, the  $\mathbb{Z}_2$  topological invariant regarding a line node is well defined by using mirror-reflection symmetry instead of spatial-inversion symmetry. The relation between the topological invariant and surface states is also discussed. When the spin-orbit interaction is switched on, the line node disappears and the system turns into a topological insulator. We investigate the topological phase of  $\text{CaAgX}$  both from the energy dispersion on the surface and from the  $\mathbb{Z}_2$  topological invariants, which is obtained to be  $\nu_0; \nu_1\nu_2\nu_3 = 1;000$ .

**Bulk electronic states.**— First, we perform the first-principles calculations by using the WIEN2k code.<sup>43,44</sup> We use the experimental structural parameters<sup>41</sup> for the calculations. Figure 1(b) shows the calculated band structures of  $\text{CaAgP}$  without the spin-orbit interaction. The line node is observed within 10 K from the Fermi level along the  $\Gamma M$  and  $\Gamma K$  lines, and it forms a circle in the  $k_x$ - $k_y$  plane centered at the  $\Gamma$  point, as illustrated in the inset of Fig. 1(b). The band dispersion at the line node is linear along both the radial and  $k_z$

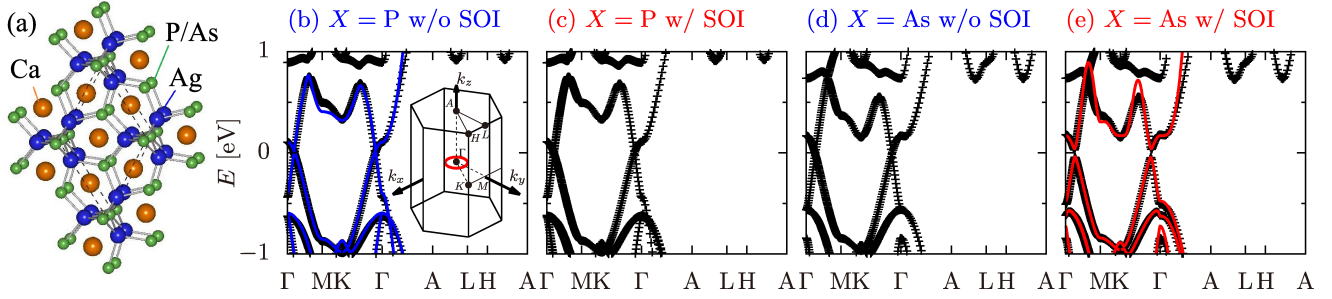


**Fig. 1.** (a) Crystal structure of  $\text{CaAgX}$  ( $X = \text{P, As}$ ). Small, middle, and large spheres represent  $X$ ,  $\text{Ag}$ , and  $\text{Ca}$  atoms, respectively. The dotted lines show the hexagonal unit cell. (b)–(e) Electronic states of  $\text{CaAgP}$  and  $\text{CaAgAs}$  with (w/) and without (w/o) spin-orbit interaction (SOI). The crosses in (b)–(e) and the solid curves in (b) and (e) indicate the band dispersion obtained by first-principles calculations and by using the tight-binding models, respectively. In the inset of (b), the location of the line node is indicated by the (red) circle around the  $\Gamma$  point in the Brillouin zone.

directions. This line node is not protected for the spin-orbit interaction. However, as shown in Fig. 1(c), the effect of the spin-orbit interaction in  $\text{CaAgP}$  is negligible and the size of the induced gap at the line node is of the order of 10 K because of the weak spin-orbit interaction in the P atom. In stark contrast, the spin-orbit interaction has a significant effect on the band structures of  $\text{CaAgAs}$ . We show the calculated band structure of  $\text{CaAgAs}$  without and with spin-orbit interaction in Figs. 1(d) and 1(e), respectively. The line node has a large gap of  $\sim 1000$  K, indicating that the bulk system is an insulator.

Next, we derive tight-binding models for  $\text{CaAgP}$  and  $\text{CaAgAs}$  to investigate the surface electronic states. According to first-principles calculations, the main component of the conduction band at the  $\Gamma$  point is the  $p_z$  ( $A_2''$  in  $D_{3h}$ ) orbital of P or As atoms. In contrast, the valence band around the  $\Gamma$  point mainly consists of the  $s$  orbital ( $A_1'$  in  $D_{3h}$ ) of Ag atoms in addition to the  $p_x$  and  $p_y$  orbitals ( $E'$  in  $D_{3h}$ ) of P or As atoms. Therefore, we construct the 12-orbital tight-binding models by constructing the maximally localized Wannier functions for the  $3p$  ( $4p$ ) orbitals of three P (As) atoms and the  $5s$  orbital of three Ag atoms in  $\text{CaAgP}$  ( $\text{CaAgAs}$ ).<sup>45,46</sup> Furthermore, we have checked that the results do not alter even if the  $d$  orbitals of Ca atoms are taken into account.<sup>47</sup> Here, the spin-orbit interaction  $H_{\text{SO}} = \lambda \mathbf{L} \cdot \mathbf{S}$ , with  $\lambda = 0.07$  eV for  $4p$  electrons, is taken into account in the  $\text{CaAgAs}$  model, whereas it is neglected in the  $\text{CaAgP}$  model. In Figs. 1(b) and 1(e), we see a good agreement between the first principle band and the obtained tight-binding band.

**Topological line node and surface states in  $\text{CaAgP}$ .**— Figure 2(a) shows the angle-resolved density of states, calculated from the surface Green's function via the QZ decomposition,<sup>48,49</sup> on the (0001) surface terminated at a  $\text{Ca}_3\text{P}$  layer. Note that two types of termination,  $\text{Ca}_3\text{X}$  and  $\text{Ag}_3\text{X}_2$ , are possible on the (0001) surface of  $\text{CaAgX}$ . Hereafter, we focus only on the former type of termination.<sup>50</sup> One can clearly see that a line node is located around the  $\bar{\Gamma}$  point, which is projected from the bulk line node, and there exist surface states within the node.

The bulk line node is protected by mirror-reflection sym-

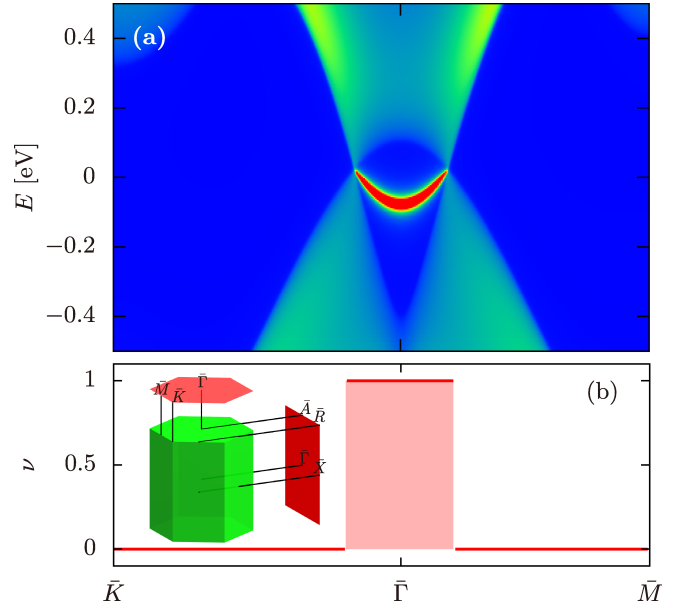


**Fig. 2.** Angle-resolved density of states on the (0001) surface with the  $\text{Ca}_3\text{P}$  termination (a) and the topological number  $\nu$  of  $\text{CaAgP}$  (b). The inset in (b) shows the projected Brillouin zones onto the (0001) and  $(10\bar{1}0)$  surfaces.

metry with respect to the horizontal plane:  $H(k_x, k_y, k_z) = M^\dagger H(k_x, k_y, -k_z)M$ . The conduction and valence bands belong to  $A_2''$  and  $A_1'$  representations, respectively; therefore, these bands are degenerate on the mirror-reflection invariant plane of  $k_z = 0$ . Mirror-reflection symmetry allows one to introduce the  $\mathbb{Z}_2$  topological invariant  $\nu$  to characterize the band inversion as

$$(-1)^{\nu(k_x, k_y)} = \xi(k_x, k_y, 0)\xi(k_x, k_y, \pi). \quad (1)$$

Here,  $\xi(\mathbf{k})$  is the product of eigenvalues of the mirror reflection for all the occupied bands at  $\mathbf{k}$ . Obviously,  $\nu(k_x, k_y) = 1$  indicates band inversion from  $k_z = 0$  to  $k_z = \pi$ . Moreover, it is worth mentioning that  $\nu(k_x, k_y)$  is related to the Berry phase:<sup>51</sup>

$$(-1)^{\nu(k_x, k_y)} = \exp \left[ i \int_{-\pi}^{\pi} dk_z \text{tr} A_z(\mathbf{k}) + \text{tr} \ln B(k_x, k_y) \right], \quad (2)$$

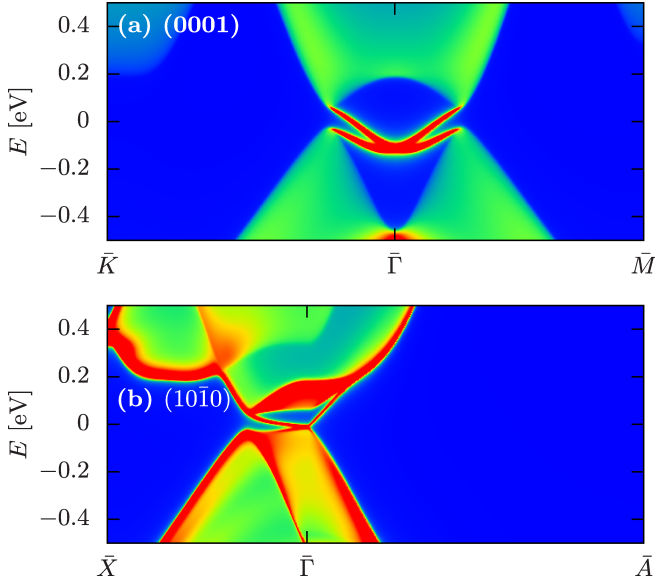


**Fig. 3.** Angle-resolved density of states on the (a) Ca<sub>3</sub>As-terminated (0001) and (b) (10 $\bar{1}$ 0) surfaces of CaAgAs.

where the non-Abelian Berry connection is defined by

$$[A(\mathbf{k})]_{mn} = -i\langle \mathbf{k}, m | \frac{\partial}{\partial \mathbf{k}} | \mathbf{k}, n \rangle, \quad (3)$$

where  $|\mathbf{k}, m\rangle$  denotes an occupied eigenstate.  $B(k_x, k_y)$  is the sewing matrix defined by

$$[B(k_x, k_y)]_{mn} = \langle (k_x, k_y, \pi), m | B_z | (k_x, k_y, \pi) - \mathbf{G}_z, n \rangle, \quad (4)$$

where  $B_j$  is an operator satisfying

$$H(\mathbf{k}) = B_j^\dagger H(\mathbf{k} + \mathbf{G}_j) B_j, \quad (5)$$

and  $\mathbf{G}_j = 2\pi\hat{x}_j$  denotes the  $j$ -th reciprocal lattice vector. The calculated  $\nu(k_x, k_y)$  is shown in Fig. 2(b). The topological invariant is obtained to be nontrivial,  $\nu(k_x, k_y) = 1$ , within the line node, while trivial,  $\nu(k_x, k_y) = 0$ , in the outside. Since  $\nu(k_x, k_y)$  is invariant for a continuous change of parameters of the Hamiltonian, the line node is a topologically stable object.

**Topological insulating phase in CaAgAs.**— The degeneracy in dihedral point-group symmetry is lifted by the spin-orbit interaction. Correspondingly, the product of the eigenvalues of mirror reflection is always unity:  $\xi(k_x, k_y, 0)\xi(k_x, k_y, \pi) = 1$ ; namely, the  $\mathbb{Z}_2$  invariant takes the trivial value  $\nu(k_x, k_y) = 0$ .<sup>52</sup> This means that the spin-orbit interaction yields an energy gap in the line node. Furthermore, the spin-orbit interaction gives rise to a transition from a line-node semimetal to a topological insulator. Figure 3 shows the angle-resolved density of states on the (0001) and (10 $\bar{1}$ 0) surfaces. In the spin-orbit gap ( $\sim 0.1$  eV), gapless surface states appear. The Dirac point is located at the  $\bar{\Gamma}$  point. On the (0001) surface [Fig. 3(a)], the gapless surface states are smoothly deformed from those in the absence of spin-orbit interaction [Fig. 2(a)]. On the (10 $\bar{1}$ 0) surface, gapless surface states with approximately linear dispersion emerge in the induced band

**Table I.** Berry phase  $\Phi_{jli\eta}(k_l)$  and  $\mathbb{Z}_2$  invariant  $\nu_{li\eta}$  of CaAgAs.

$i$	1	1	2	2	3	3
$\eta$	0	1	0	1	0	1
$\Phi_{jli\eta}(k_l = 0)$	$2\pi$	0	$2\pi$	0	$2\pi$	0
$\Phi_{jli\eta}(k_l = \pi)$	0	0	0	0	0	0
$\nu_{li\eta}$	1	0	1	0	1	0

gap. The in-plane ( $\bar{\Gamma}\bar{X}$ ) velocity of the surface Dirac fermion is slower than the out-of-plane ( $\bar{\Gamma}\bar{A}$ ) one, since the lattice constant along the  $c$  axis is so small ( $c/a \sim 0.6$ ) that the interlayer coupling is much stronger.

The obtained gapless surface states, shown in Fig. 3, coincide with the  $\mathbb{Z}_2$  topological invariants of  $\nu_0; \nu_1\nu_2\nu_3 = 1; 000$ . The simplified formula for the invariant derived by Fu and Kane<sup>53</sup> cannot be applied to the present system owing to the lack of spatial-inversion symmetry. Instead, with the help of mirror-reflection symmetries with respect to the horizontal  $H(k_x, k_y, k_z) = M_z^\dagger H(k_x, k_y, k_z) M_z$  and the vertical  $H(k_x, k_y, k_z) = M_y^\dagger H(k_x, -k_y, k_z) M_y$  planes, the topological invariants can be easily calculated as

$$\nu_{li\eta} = \frac{\Phi_{jli\eta}(k_l = 0) + \Phi_{jli\eta}(k_l = \pi)}{2\pi} \pmod{2}, \quad (6)$$

for  $i, j, l = 1, 2, 3$  ( $i \neq j \neq l \neq i$ ) and  $\eta = 0, 1$ .<sup>54</sup> The  $\mathbb{Z}_2$  topological invariants are obtained by  $\nu_0 = \nu_{i0} + \nu_{i1} \pmod{2}$ ,  $\nu_i = \nu_{i1}$ . The Berry phase is given by

$$\Phi_{jli\eta}(k_l) = \int_{-\pi}^{\pi} dk_j \text{tr} A_j(\mathbf{k})|_{k_i=\eta\pi} - i \text{tr} \ln B_{jli\eta}(k_l), \quad (7)$$

where  $B_{jli\eta}(k_l)$  is the sewing matrix defined by

$$[B_{jli\eta}(k_l)]_{mn} = \langle \mathbf{k}, m | B_j | \mathbf{k} - \mathbf{G}_j, n \rangle|_{k_j=\pi, k_i=\eta\pi}. \quad (8)$$

Formula (7) is useful because only two points  $k_l = 0$  and  $k_l = \pi$  are needed for the calculation, as in the case of spatial-inversion invariant systems.<sup>30</sup> The calculated Berry phases are summarized in Table I. All the Berry phases on the zone boundaries  $k_i = \pi$  are zero, resulting in the topological invariants of 1; 000.<sup>55</sup>

**Effective model.**— We now derive effective models for CaAgP and CaAgAs. In the model of CaAgAs (CaAgP), we (do not) take into account the spin-orbit interaction.

As discussed above, the conduction and valence bands at the  $\Gamma$  point of CaAgP mainly consist of the  $A_2''$  and  $A_1'$  states, respectively. Thus, the low-energy electronic structure is effectively described by the two-band model

$$H_{\text{CaAgP}}(\mathbf{k}) = c(\mathbf{k}) + m(\mathbf{k})\sigma_z + vk_z\sigma_y, \quad (9)$$

with  $c(\mathbf{k}) = c_0 + c_1k_z^2 + c_2(k_x^2 + k_y^2)$  and  $m(\mathbf{k}) = m_0 + m_1k_z^2 + m_2(k_x^2 + k_y^2)$  in the vicinity of the  $\Gamma$  point. A line node appears on the  $k_z = 0$  plane under the band-inversion condition of  $m_0m_2 < 0$ .

In CaAgAs, the four-fold degenerated valence-band states at the  $\Gamma$  point without the spin-orbit interaction, which consist of  $E'$  states, are split into two doublets ( $E_{3/2}$  and  $E_{5/2}$ ) by in-

roducing the spin-orbit interaction. The resulting low-energy states consist of the  $E_{5/2}$  doublet in the valence band and the  $E_{3/2}$  doublet in the conduction band, which are described by the Hamiltonian

$$H_{\text{CaAgAs}}(\mathbf{k}) = \begin{pmatrix} h(\mathbf{k}) & \Lambda(\mathbf{k}) \\ \Lambda(\mathbf{k})^\dagger & h(-\mathbf{k})^* \end{pmatrix}. \quad (10)$$

$h(\mathbf{k})$  is the  $2 \times 2$  Hamiltonian matrix for the states in which the  $z$  components of the total angular momentum are given by  $j_z = 1/2$  and by  $j_z = 3/2$ .  $h(\mathbf{k})$  reads

$$h(\mathbf{k}) = c(\mathbf{k}) + m(\mathbf{k})\sigma_z + Ak_z(k_x\sigma_x - k_y\sigma_y), \quad (11)$$

up to the second order of  $k$ .  $\Lambda(\mathbf{k})$  is the  $2 \times 2$  matrix representing the spin-mixing effect induced by the spin-orbit interaction, defined by  $\Lambda(\mathbf{k}) = \Lambda_1(\mathbf{k}) + \Lambda_2(\mathbf{k})$ , where

$$\Lambda_1(\mathbf{k}) = -iB_\perp k_z(1 - \sigma_z) + -iB_\parallel(k_x + ik_y)\sigma_x, \quad (12)$$

$$\Lambda_2(\mathbf{k}) = D\sigma_y \left[ -i(k_x^2 - k_y^2) - 2k_x k_y \right]. \quad (13)$$

$\Lambda(\mathbf{k})$  yields a finite energy gap on the  $k_z = 0$  plane, thereby turning the system into a strong topological insulator with 1;000.

These two effective Hamiltonians qualitatively describe the electronic structures of CaAgP and CaAgAs. Therefore, it is useful for a further analysis of the electromagnetic responses and transport properties of these materials. These Hamiltonians, however, do not quantitatively reproduce the low-energy electronic states, because the line node is located rather far from the  $\Gamma$  point. To obtain a quantitatively good model, one has to take into account higher energy states in addition to the low-lying states.

**Summary.**— We have clarified the topological electronic structure of hexagonal pnictides CaAgX ( $X = \text{P}$  and  $\text{As}$ ). CaAgX is a line-node Dirac semimetal in the absence of spin-orbit interaction. In reality, CaAgP exhibits line-node-semimetal properties except in the very low energy and low-temperature regime owing to the tiny spin-orbit interaction ( $\sim 10$  K). When P atoms are replaced with heavier As atoms, the strong spin-orbit interaction widens the size of the band gap considerably at the line node. CaAgAs is found to be a strong topological insulator with the  $\mathbb{Z}_2$  invariant of 1;000.

It has been known that the presence of reflection symmetry and band inversion is necessary and sufficient for the existence of a line node, whereas most of the line-node Dirac semimetals proposed so far preserve spatial-inversion symmetry. Moreover, the  $\mathbb{Z}_2$  topological invariant characterizing the line node was defined in previous works in terms of  $PT$  symmetry.<sup>15,25</sup> This invariant cannot be directly applied to systems lacking inversion symmetry, including CaAgX reported here. We have introduced the alternative  $\mathbb{Z}_2$  invariant  $\nu(k_x, k_y)$  in this study, which is applicable to systems without spatial-inversion symmetry. This implies that line-node Dirac semimetals with and without spatial-inversion symmetry might exhibit intrinsically different electromagnetic responses and transport phenomena, which are related to the topological invariants. Superconductivity of line-node

semimetals is another interesting topic, as discussed in point-node Weyl<sup>56–61</sup> and Dirac semimetals.<sup>62</sup> These issues will be addressed in future works.

**Note added.**— After the submission of this paper, we became aware of a recent preprint<sup>63</sup> in which the relation between the Berry phase and eigenvalues of mirror reflection is discussed in a form different from Eqs. (1) and (2).

**Acknowledgment** The authors are grateful to S. Kobayashi for valuable discussion.

- 1) D. J. Thouless, M. Kohmoto, M. P. Nightingale, and M. den Nijs: Phys. Rev. Lett. **49** (1982) 405.
- 2) M. Kohmoto: Ann. Phys. **160** (1985) 343.
- 3) M. Z. Hasan and C. L. Kane: Rev. Mod. Phys. **82** (2010) 3045.
- 4) X.-L. Qi and S.-C. Zhang: Rev. Mod. Phys. **83** (2011) 1057.
- 5) Y. Tanaka, M. Sato, and N. Nagaosa: J. Phys. Soc. Jpn. **81** (2012) 011013.
- 6) S. Murakami: New J. Phys. **9** (2007) 356.
- 7) X. Wan, A. M. Turner, A. Vishwanath, and S. Y. Savrasov: Phys. Rev. B **83** (2011) 205101.
- 8) S. M. Young, S. Zaheer, J. C. Y. Teo, C. L. Kane, E. J. Mele, and A. M. Rappe: Phys. Rev. Lett. **108** (2012) 140405.
- 9) J. A. Steinberg, S. M. Young, S. Zaheer, C. L. Kane, E. J. Mele, and A. M. Rappe: Phys. Rev. Lett. **112** (2014) 036403.
- 10) K. Fukushima, D. E. Kharzeev, and H. J. Warringa: Phys. Rev. D **78** (2008) 074033.
- 11) A. A. Zyuzin, S. Wu, and A. A. Burkov: Phys. Rev. B **85** (2012) 165110.
- 12) P. Hosur and X. Qi: Compt. Rend. Phys. **14** (2013) 857.
- 13) A. A. Burkov, M. D. Hook, and L. Balents: Phys. Rev. B **84** (2011) 235126.
- 14) C.-K. Chiu and A. P. Schnyder: Phys. Rev. B **90** (2014) 205136.
- 15) C. Fang, Y. Chen, H.-Y. Kee, and L. Fu: Phys. Rev. B **92** (2015) 081201.
- 16) Z. Gao, M. Hua, H. Zhang, and X. Zhang: arXiv:1507.07504.
- 17) G. P. Mikitik and Y. V. Sharlai: Phys. Rev. B **73** (2006) 235112.
- 18) T. T. Heikkilä and G. E. Volovik: JETP Lett. **93** (2011) 59.
- 19) T. T. Heikkilä and G. E. Volovik: arXiv:1505.03277.
- 20) M. Phillips and V. Aji: Phys. Rev. B **90** (2014) 115111.
- 21) K. Mullen, B. Uchoa, and D. T. Glatzhofer: Phys. Rev. Lett. **115** (2015) 026403.
- 22) H. Weng, C. Fang, Z. Fang, B. A. Bernevig, and X. Dai: Phys. Rev. X **5** (2015) 011029.
- 23) H. Weng, Y. Liang, Q. Xu, R. Yu, Z. Fang, X. Dai, and Y. Kawazoe: Phys. Rev. B **92** (2015) 045108.
- 24) Y. Chen, Y. Xie, S. A. Yang, H. Pan, F. Zhang, M. L. Cohen, and S. Zhang: arXiv:1505.02284.
- 25) Y. Kim, B. J. Wieder, C. L. Kane, and A. M. Rappe: Phys. Rev. Lett. **115** (2015) 036806.
- 26) R. Yu, H. Weng, Z. Fang, X. Dai, and X. Hu: Phys. Rev. Lett. **115** (2015) 036807.
- 27) M. Zeng, C. Fang, G. Chang, Y.-A. Chen, T. Hsieh, A. Bansil, H. Lin, and L. Fu: arXiv:1504.03492.
- 28) J.-M. Carter, V. V. Shankar, M. A. Zeb, and H.-Y. Kee: Phys. Rev. B **85** (2012) 115105.
- 29) Y. Chen, Y.-M. Lu, and H.-Y. Kee: Nature Communications **6** (2015) 6593.
- 30) H.-S. Kim, Y. Chen, and H.-Y. Kee: Phys. Rev. B **91** (2015) 235103.
- 31) J. Liu, D. Krieger, L. Horak, D. Puggioni, C. Rayan Serrao, R. Chen, D. Yi, C. Frontera, V. Holy, A. Vishwanath, J. M. Rondinelli, X. Marti, and R. Ramesh: arXiv:1506.03559.
- 32) J.-W. Rhim and Y. B. Kim: Phys. Rev. B **92** (2015) 045126.
- 33) Y. Huh, E.-G. Moon, and Y. B. Kim: arXiv:1506.05105.
- 34) A. K. Mitchell and L. Fritz: arXiv:1506.05491.
- 35) S. T. Ramamurthy and T. L. Hughes: arXiv:1508.01205.

- 36) L. S. Xie, L. M. Schoop, E. M. Seibel, Q. D. Gibson, W. Xie, and R. J. Cava: *APL Mater.* **3** (2015) 083602.
- 37) G. Bian, T.-R. Chang, R. Sankar, S.-Y. Xu, H. Zheng, T. Neupert, C.-K. Chiu, S.-M. Huang, G. Chang, I. Belopolski, D. S. Sanchez, M. Neupane, N. Alidoust, C. Liu, B. Wang, C.-C. Lee, H.-T. Jeng, A. Bansil, F. Chou, H. Lin, and M. Zahid Hasan: arXiv:1505.03069 .
- 38) L. M. Schoop, M. N. Ali, C. Straßer, V. Duppe, S. S. P. Parkin, B. V. Lotsch, and C. R. Ast: arXiv:1509.00861 .
- 39) L. Lu, L. Fu, J. D. Joannopoulos, and M. Soljačić: *Nat. Photo.* **7** (2013) 294.
- 40) W. M. H. Natori, E. Miranda, and R. G. Pereira: arXiv:1505.06171 .
- 41) A. Mewis: *Zeitschrift für Naturforschung B* **34** (1979) 14.
- 42) H. Ishikawa, T. Okubo, Y. Okamoto, and Z. Hiroi: *J. Phys. Soc. Jpn.* **83** (2014) 043703.
- 43) P. Blaha, K. Schwarz, G. Madsen, D. Kvasnicka, and J. Luitz: *WIEN2k, An Augmented Plane Wave + Local Orbitals Program for Calculating Crystal Properties* (Techn. Universität Wien, Austria, 2001).
- 44) We used the full-potential linearized augmented plane-wave method within the generalized gradient approximation as implemented in the WIEN2k code.<sup>43</sup>  $24 \times 24 \times 36$   $k$ -points sampling was used for the self-consistent calculation.
- 45) N. Marzari and D. Vanderbilt: *Phys. Rev. B* **56** (1997) 12847.
- 46) I. Souza, N. Marzari, and D. Vanderbilt: *Phys. Rev. B* **65** (2001) 035109.
- 47) See Sec. S 4 of Supplemental Material.
- 48) T. Miyata, S. Honda, R. Naito, and S.-L. Zhang: *Jpn. J. Ind. Appl. Math.* **30** (2013) 653.
- 49) T. Miyata, R. Naito, and S. Honda: *J. Eng. Math.* (2015) 1.
- 50) Electronic states on the  $\text{Ag}_3\text{X}_2$  termination is shown in Sec. S 1 of Supplemental Material.
- 51) Equation (1) is derived from Eq. (2). See Sec. S 2 of Supplemental Material.
- 52) See Sec. S 2.4 of Supplemental Material.
- 53) L. Fu and C. L. Kane: *Phys. Rev. B* **76** (2007) 045302.
- 54) Equation (6) is obtained for mirror-reflection-invariant systems. See Sec. S 3 of Supplemental Material.
- 55) Dirac semimetals in which a line node is located around the  $\Gamma$  point always becomes a strong topological insulator with  $\nu_0; \nu_1 \nu_2 \nu_3 = 1; 000$  when spin-orbit interaction is switched on. See Sec. S 3.3 of Supplemental Material.
- 56) G. Y. Cho, J. H. Bardarson, Y.-M. Lu, and J. E. Moore: *Phys. Rev. B* **86** (2012) 214514.
- 57) V. Shivamoggi and M. J. Gilbert: *Phys. Rev. B* **88** (2013) 134504.
- 58) H. Wei, S.-P. Chao, and V. Aji: *Phys. Rev. B* **89** (2014) 014506.
- 59) H. Wei, S.-P. Chao, and V. Aji: *Phys. Rev. B* **89** (2014) 235109.
- 60) B. Lu, K. Yada, M. Sato, and Y. Tanaka: *Phys. Rev. Lett.* **114** (2015) 096804.
- 61) G. Bednik, A. A. Zyuzin, and A. A. Burkov: *Phys. Rev. B* **92** (2015) 035153.
- 62) S. Kobayashi and M. Sato: arXiv:1504.07408 .
- 63) Y.-H. Chan, C.-K. Chiu, M. Y. Chou, and A. P. Schnyder: arXiv:1510.02759 .
- 64) S. Kobayashi *et al.*, in preparation.
- 65) R. Yu, X. L. Qi, A. Bernevig, Z. Fang, and X. Dai: *Phys. Rev. B* **84** (2011) 075119.
- 66) L. Fu and E. Berg: *Phys. Rev. Lett.* **105** (2010) 097001.
- 67) X.-L. Qi, T. L. Hughes, and S.-C. Zhang: *Phys. Rev. B* **81** (2010) 134508.
- 68) M. Sato: *Phys. Rev. B* **81** (2010) 220504.

## S 1. Termination-dependent (0001) surface states

$\text{CaAgX}$  consists of alternating stacking of  $\text{Ca}_3\text{X}$  and  $\text{Ag}_3\text{X}_2$  layers along the  $c$  axis, i.e., the (0001) surface can be terminated by either of these layers. Correspondingly, energy dispersion relations of (0001) surface states on the  $\text{Ca}_3\text{X}$  termination are different from those on the  $\text{Ag}_3\text{X}_2$  termination.

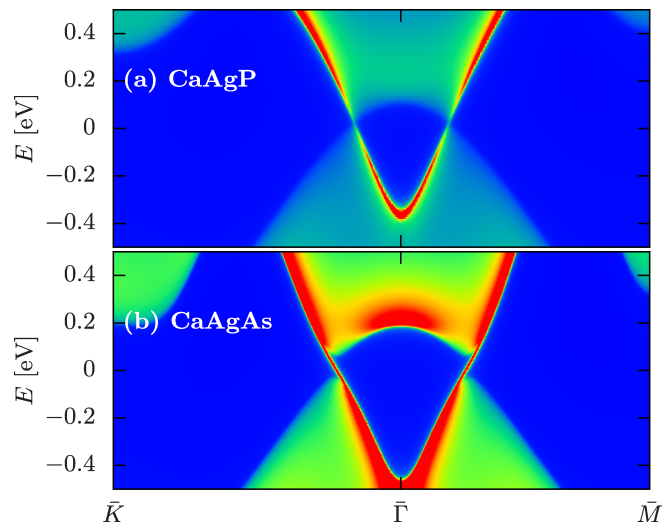


**Fig. S 1.** Angle-resolved density of states on the (0001) surface with the  $\text{Ag}_3\text{X}_2$  termination for  $X = \text{P}$  (a),  $\text{As}$  (b).

Angle-resolve density of states on the  $\text{Ag}_3\text{X}_2$  termination is shown in Fig. S 1. Surface states on the  $\text{Ca}_3\text{X}$  termination of  $\text{CaAgP}$  ( $\text{CaAgAs}$ ) show up within the (gapped) line node, as shown in Fig. 2(a) [3(a)], while those on the  $\text{Ag}_3\text{X}_2$  termination do not, as shown in Fig. S 1.

## S 2. $\mathbb{Z}_2$ line node protected by mirror-reflection symmetry

A line node protected by mirror-reflection symmetry is simply understood as follows: conduction and valence bands have opposite parity of the reflection hence these are degenerated at the reflection invariant plane  $k_z = 0$  or  $k_z = \pi$ . Here, we show that the topological invariant which is associated with a line node can be defined in terms of Berry phase.

### S 2.1 Definition

Suppose a system preserving mirror-reflection symmetry with respect to the horizontal plane. The Hamiltonian  $H(\mathbf{k})$  satisfies

$$H(k_x, k_y, k_z) = M^\dagger H(k_x, k_y, -k_z)M. \quad (\text{S14})$$

Mirror-reflection operator  $M$ , in general, depends on  $k_z$  in systems with sublattice structure. In the following, we choose the gauge in which  $M$  is independent of  $k_z$ . Instead, the Hamiltonian has a nontrivial periodicity:

$$H(\mathbf{k}) = B^\dagger H(\mathbf{k} + \mathbf{G}_z)B, \quad (\text{S15})$$

where  $\mathbf{G}_z = (0, 0, 2\pi)$  denotes the reciprocal lattice vector along the  $z$  axis. The  $\mathbb{Z}_2$  topological invariant  $\nu(k_x, k_y)$  is defined by

$$(-1)^{\nu(k_x, k_y)} = \exp \left[ i \int_{-\pi}^{\pi} dk_z \text{tr} A_z(\mathbf{k}) + \text{tr} \ln B(k_x, k_y) \right]. \quad (\text{S16})$$

The non-Abelian Berry connection  $A(\mathbf{k})$  and unitary matrix  $B(k_x, k_y)$  are defined by

$$[A(\mathbf{k})]_{mn} = -i\langle \mathbf{k}, m | \frac{\partial}{\partial \mathbf{k}} | \mathbf{k}, n \rangle, \quad (\text{S17})$$

and

$$[B(k_x, k_y)]_{mn} = \langle (k_x, k_y, \pi), m | B | (k_x, k_y, -\pi), n \rangle. \quad (\text{S18})$$

### S 2.2 Gauge symmetry

Next, we show that  $\nu(k_x, k_y) \bmod 2$  is invariant under a  $U(N)$  gauge transformation  $|\mathbf{k}, m\rangle \rightarrow |\mathbf{k}, n\rangle [g(\mathbf{k})]_{nm}$ ,  $g(\mathbf{k}) \in U(N)$ .  $A(\mathbf{k})$  and  $B(k_x, k_y)$  are transformed into

$$A(\mathbf{k}) \rightarrow g^\dagger(\mathbf{k}) A(\mathbf{k}) g(\mathbf{k}) - i g^\dagger(\mathbf{k}) \frac{\partial g(\mathbf{k})}{\partial \mathbf{k}}, \quad (\text{S19})$$

$$B(k_x, k_y) \rightarrow g^\dagger(k_x, k_y, \pi) B(k_x, k_y) g(k_x, k_y, -\pi). \quad (\text{S20})$$

From the integral

$$\int_{-\pi}^{\pi} dk_z \text{tr} g^\dagger(\mathbf{k}) \frac{\partial g(\mathbf{k})}{\partial k_z} = \ln \frac{\det g(k_x, k_y, \pi)}{\det g(k_x, k_y, -\pi)} + i2n\pi, \quad n \in \mathbb{Z}, \quad (\text{S21})$$

one can verify that the right hand side of Eq. (S16) is invariant under the gauge transformation.

### S 2.3 $\mathbb{Z}_2$ invariant and mirror-reflection symmetry

If the system has mirror-reflection symmetry,  $\nu(k_x, k_y)$  is the  $\mathbb{Z}_2$  invariant. The mirror-reflection symmetry requires the following relation;

$$H(k_x, k_y, k_z) = M^\dagger H(k_x, k_y, -k_z) M. \quad (\text{S22})$$

We introduce the unitary matrix  $M(\mathbf{k})$  in the occupied subspace;

$$[M(k_x, k_y, k_z)]_{mn} = \langle (k_x, k_y, k_z), m | M | (k_x, k_y, -k_z), n \rangle. \quad (\text{S23})$$

On the reflection invariant plane of  $k_z = 0$ , the states are simultaneously the eigenstates of  $M$  hence

$$\det M(k_x, k_y, 0) = \pm 1, \quad (\text{S24})$$

where the phase of  $M$  is fixed as  $M^2 = 1$ . On the other reflection invariant plane of  $k_z = \pi$ , the mirror-reflection operator is modified to

$$M' = M B^\dagger. \quad (\text{S25})$$

$M'$  satisfies

$$[H(k_x, k_y, \pi), M'] = 0. \quad (\text{S26})$$

Unitary matrix defined by

$$[M'(k_x, k_y, \pi)]_{mn} = \langle (k_x, k_y, \pi), m | M' | (k_x, k_y, \pi), n \rangle, \quad (\text{S27})$$

also satisfies

$$\det M'(k_x, k_y, \pi) = \pm 1. \quad (\text{S28})$$

Now we prove that  $\nu(k_x, k_y)$  is the  $\mathbb{Z}_2$  invariant. The non-

Abelian Berry connection satisfies

$$A_z(k_x, k_y, k_z) = -M^\dagger(k_x, k_y, -k_z) A_z(k_x, k_y, -k_z) M(k_x, k_y, -k_z) + i M^\dagger(k_x, k_y, -k_z) \frac{\partial M(k_x, k_y, -k_z)}{-\partial k_z}. \quad (\text{S29})$$

Therefore, the integral of  $A$  reduces to

$$\int_{-\pi}^0 dk_z \text{tr} A_z(\mathbf{k}) = - \int_0^\pi dk_z \text{tr} A_z(\mathbf{k}) + i \int_0^\pi dk_z \text{tr} M^\dagger(\mathbf{k}) \frac{\partial M(\mathbf{k})}{\partial k_z}. \quad (\text{S30})$$

The second term is rewritten as

$$i \int_0^\pi dk_z \text{tr} M^\dagger(\mathbf{k}) \frac{\partial M(\mathbf{k})}{\partial k_z} = i \ln \frac{\det M(k_x, k_y, \pi)}{\det M(k_x, k_y, 0)} + 2n\pi. \quad (\text{S31})$$

Consequently, one obtains

$$i \int_{-\pi}^{\pi} dk_z \text{tr} A_z(\mathbf{k}) + \text{tr} \ln B(k_x, k_y) = - \ln \frac{\det M'(k_x, k_y, \pi)}{\det M(k_x, k_y, 0)} + i2n\pi, \quad (\text{S32})$$

namely

$$(-1)^{\nu(k_x, k_y)} = \frac{\det M'(k_x, k_y, \pi)}{\det M(k_x, k_y, 0)} = \pm 1, \quad (\text{S33})$$

which is the same as Eq. (1) in the main manuscript.

### S 2.4 Topological invariant in spinful systems

In spinful systems, the topological invariants of spin up and down may cancel each other out;  $\nu(k_x, k_y) = 0$ , owing to time-reversal  $T$  symmetry. The mirror reflection in spinful systems involves the spin hence  $T^{-1} M T = -M$ , and

$$M(\mathbf{k})^* = -T(-\mathbf{k})^\dagger M(-\mathbf{k}) T(-\mathbf{k}), \quad (\text{S34})$$

where unitary skew matrix  $T(\mathbf{k})$  is defined by

$$[T(\mathbf{k})]_{mn} = \langle \mathbf{k}, m | T | -\mathbf{k}, n \rangle. \quad (\text{S35})$$

As a result, one obtains

$$\text{tr} M(k_x, k_y, 0) = -\text{tr} M(-k_x, -k_y, 0), \quad (\text{S36})$$

$$\text{tr} M'(k_x, k_y, \pi) = -\text{tr} M'(-k_x, -k_y, \pi). \quad (\text{S37})$$

For  $(k_x, k_y, \Gamma)$ ,  $\Gamma = 0, \pi$ , which is continuously connected (without gap closing) to a time-reversal invariant momentum  $\Gamma$  within the  $k_z = \Gamma$  plane, the following relation holds

$$\text{tr} M(k_x, k_y, 0) = \text{tr} M'(k_x, k_y, \pi) = 0, \quad (\text{S38})$$

since  $\text{tr} M(\Gamma) = \text{tr} M'(\Gamma) = 0$  and  $\text{tr} M(k_x, k_y, \Gamma)$  is a quantized invariant. Consequently, the number of occupied states with the eigenvalue of  $+i$  of mirror reflection are the same as that with the eigenvalue of  $-i$ . This proves that  $\det M(k_x, k_y, 0) = \det M(k_x, k_y, \pi) = (-1)^{N/2}$ ,  $\nu(k_x, k_y) = 0$ , where  $N$  denotes the number of occupied bands, and that there is no line node encircling time-reversal invariant momenta. Note that line nodes not around time-reversal invariant momenta may appear in a case that antisymmetric spin-orbit interaction is much stronger than symmetric one,<sup>64</sup> nevertheless it is not the case in an actual material CaAgX.

### S 3. $\mathbb{Z}_2$ invariant and mirror-reflection symmetry in the presence of spin-orbit interaction

We show that the  $\mathbb{Z}_2$  invariant characterizing insulators which respect both time-reversal and mirror-reflection symmetries reduces to the one-dimensional topological invariant Eq. (1).

#### S 3.1 Definition

We start with the following expression

$$\nu = \int_0^\pi \frac{dk_y}{2\pi} \frac{\partial \Phi(k_y)}{\partial k_y} - \frac{\Phi(\pi) - \Phi(0)}{2\pi} \pmod{2}. \quad (\text{S39})$$

$\Phi(k_y)$  is the Berry phase defined by

$$\Phi(k_y) = \int_{-\pi}^\pi dk_x \text{tr} A_x(\mathbf{k}) - i \text{tr} \ln B(k_y), \quad (\text{S40})$$

with

$$[B(k_y)]_{mn} = \langle (\pi, k_y), m | B | (-\pi, k_y), n \rangle. \quad (\text{S41})$$

Operator  $B$  satisfies

$$H(k_x, k_y) = B^\dagger H(k_x + 2\pi, k_y) B. \quad (\text{S42})$$

Equations (S39) and (S40) are equivalent to the  $\mathbb{Z}_2$  invariant derived in Ref.<sup>65</sup> This is obviously confirmed in a particular choice of gauge in which  $B$  is the identity.

#### S 3.2 Mirror-reflection symmetry and reduced formula

Now we prove

$$\nu = \frac{\Phi(0) + \Phi(\pi)}{2\pi} \pmod{2}, \quad (\text{S43})$$

in the presence of mirror-reflection symmetry as

$$H(k_x, k_y) = M^\dagger H(-k_x, k_y) M. \quad (\text{S44})$$

In a manner similar to Secs. S 2.3 and S 2.4,  $\Phi(k_y)$  reduces to

$$\Phi(k_y) = 2n\pi, \quad n \in \mathbb{Z}. \quad (\text{S45})$$

$\Phi(k_y) \pmod{2\pi}$  for  $k_y \neq 0, \pi$  is gauge invariant, while on the time-reversal invariant momenta  $\Phi(0) \pmod{4\pi}$  and  $\Phi(\pi) \pmod{4\pi}$  are.<sup>65</sup> This means that only  $\Phi(0)$  and  $\Phi(\pi)$  determines the  $\mathbb{Z}_2$  invariant. Then we arrive at Eq. (S43).

#### S 3.3 Line node and strong topological insulator

Suppose a system hosting a line node located on the  $k_z = 0$  plane around the  $\Gamma$  point in the Brillouin zone, as in the case of CaAgX discussed in the main manuscript. Spin-orbit interaction induces an energy gap at the line node. Here we calculate the  $\mathbb{Z}_2$  topological invariant. On the  $k_x = 0$  and  $k_x = \pi$  planes, the invariant is given by

$$\nu_{1\eta} = \frac{\Phi_{321\eta}(0) + \Phi_{321\eta}(\pi)}{2\pi} \pmod{2}, \quad (\text{S46})$$

where the subscript is defined in Eq. (7). Berry phase  $\Phi_{321\eta}(\Gamma)$  is given by the integral along the  $k_z$  axis on the zone center and zone boundary, where the energy gap does not vanish as one turns off the spin-orbit interaction. From this fact, the Berry

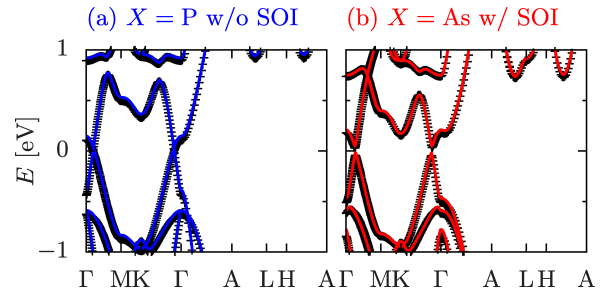


**Fig. S 2.** Bulk electronic states of (a) CaAgP without spin-orbit interaction and (b) CaAgAs with spin-orbit interaction. Energy bands obtained by using the 27-orbital tight-binding model and by first-principles calculation are denoted by the solid lines and by the crosses, respectively.

phase reduces to that in the absence of spin-orbit interaction;

$$\Phi_{321\eta}(\Gamma) = \Phi_{321\eta}^\uparrow(\Gamma) + \Phi_{321\eta}^\downarrow(\Gamma) = 2\Phi_{321\eta}^\uparrow(\Gamma), \quad (\text{S47})$$

where  $\Phi^\uparrow$  and  $\Phi^\downarrow$  denote the Berry phase in the spin-up and spin-down subspaces without spin-orbit interaction. A similar technique is found in Refs.<sup>66–68</sup> Furthermore, from Eqs. (S32) and (S33),

$$\Phi_{321\eta}(\Gamma) = 2\pi\nu(\eta\pi, \Gamma) \pmod{4\pi}. \quad (\text{S48})$$

The  $\mathbb{Z}_2$  invariant  $\nu(k_x, k_y)$  associated with a line node is obtained to be  $\nu(k_x, k_y) = 1$  [ $\nu(k_x, k_y) = 0$ ] within (out of) the line node. Therefore,  $\nu_{i\eta} = 1$  when the four time-reversal invariant momenta on the  $k_i = \eta\pi$  plane are enclosed by an odd number of line nodes, otherwise  $\nu_{i\eta} = 0$ . For instance, in the case that there is a single line node around  $\Gamma_{\text{line}} = (\Gamma_{\text{line}}^x, \Gamma_{\text{line}}^y, \Gamma_{\text{line}}^z)$ , the topological invariants are obtained to be

$$(\nu_1, \nu_2) = (\Gamma_{\text{line}}^x, \Gamma_{\text{line}}^y) / \pi, \quad \nu_0 = 1. \quad (\text{S49})$$

For the case of CaAgX, because a single line node appears around the  $\Gamma$  point, one gets

$$(\nu_1, \nu_2) = (0, 0), \quad \nu_0 = 1. \quad (\text{S50})$$

And also, one can calculate  $\nu_3$  in a similar manner since an additional mirror-reflection symmetry with respect to the  $xz$  plane is satisfied and the system has an energy gap and no integral pass along the  $k_y$  direction through the line node on the  $k_z = \pi$  plane in the absence of spin-orbit interaction, In consequence, we obtain

$$\nu_{31} = 0. \quad (\text{S51})$$

The resultant  $\mathbb{Z}_2$  invariant is given by 1;000.

### S 4. 27-orbital model

Here we show bulk and surface electronic states of a tight-binding model for CaAgX which consists of the 27 orbitals, i.e.,  $d$  orbitals of Ca,  $s$  orbitals of Ag, and  $p$  orbitals of X. Similarly to the 12-orbital model as discussed in the main context, spin-orbit interaction of CaAgP is neglected.

In CaAgAs, on the other hand, spin-orbit interaction only for the  $p$  orbitals of As atoms is taken into account in the form

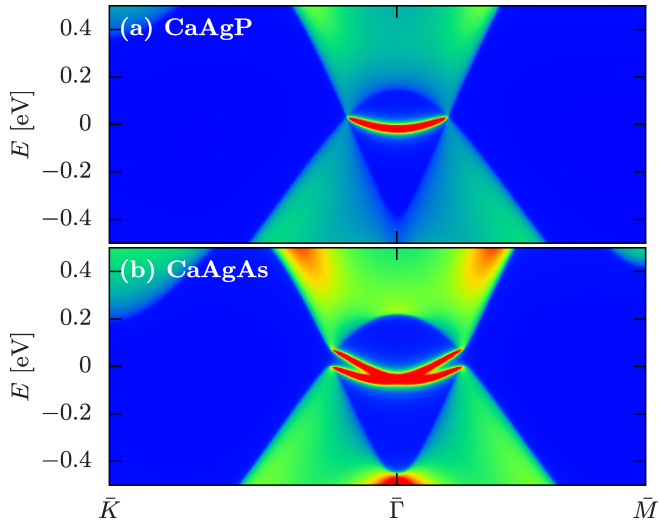


**Fig. S 3.** Angle-resolved density of states obtained by using the 27-orbital tight-binding model on the (0001) surface with the  $\text{Ca}_3X$  termination for  $X = \text{P}$  (a), As (b).

of  $H_{\text{SOI}} = \lambda \mathbf{L} \cdot \mathbf{S}$  with  $\lambda = 0.07$  eV. The bulk and surface electronic states are shown in Figs. S 2 and S 3, respectively. The obtained energy bands for both CaAgP [Fig. S 2(a)] and CaAgAs [Fig. S 2(b)] well coincide with the first-principles bands not only in the low-energy regime ( $E \sim 0$  eV) but also in high-energy regime ( $E \sim 1$  eV). The electronic states for CaAgX on the (0001) surface with  $\text{Ca}_3X$  termination are shown in Fig. S 3, which are qualitatively the same as those of the 12-orbital models shown in Figs. 2(a) and 3(a). One can confirm that the model dependence of electronic states is negligibly small.